geosciences

MDPI

Article

Lithosphere Structure of the Southern Dinarides and Continuity of the Adriatic Lithosphere Slab Beneath the Northern Dinarides Unravelled by Seismic Modelling

Franjo Šumanovac

Faculty of Mining, Geology and Petroleum Engineering, University of Zagreb, Pierottijeva 6, 10000 Zagreb, Croatia; franjo.sumanovac@rgn.hr

Abstract: Currently recognised lithospheric models hypothesise the non-existence of a lithospheric slab (a so-called slab gap) in the area of the Northern Dinarides, and the possible existence of a shallow slab in the Southern Dinarides. These geological models are mostly based on previous regional and global 3D velocity models obtained from teleseismic tomography. Recent local tomographic models providing a good resolution have regularly shown the existence of a fast anomaly underneath the entire Dinarides, directly indicating the existence of a lithospheric slab. To avoid interpretation pitfalls and increase reliability, forward seismic modelling based on new tomographic models was performed. Seismic modelling indicates a continuous lithospheric slab along the entire Dinarides in the shallow mantle, but it is not continuous vertically. In the Northern Dinarides, the shallow lithospheric slab extends at least to a depth of 150 km. In the Southern and Central Dinarides, there is a deep fast anomaly that can be interpreted in two ways due to the weak vertical resolution of teleseismic tomography. The first model suggests a steeply dipping continuous Adriatic lithospheric slab whereas the second model shows that the slab consists of two separate blocks, meaning that the deeper block was formed by delamination of the Adriatic lithospheric slab. Due to a similar correlation between the inverse velocity models for the synthetic model and the observed data, preference is not given to any model. The second model could indicate two independent Dinaridic subduction phases, as opposed to viewing subduction as a single long process during the geological past.

Keywords: teleseismic tomography; lithospheric slab; Adriatic microplate; dinarides; pannonian basin; subduction

Citation: Šumanovac, F. Lithosphere Structure of the Southern Dinarides and Continuity of the Adriatic Lithosphere Slab Beneath the Northern Dinarides Unravelled by Seismic Modelling. *Geosciences* **2022**, *12*, 439. https://doi.org/10.3390/geosciences12120439

Academic Editors: Jesus Martinez-Frias, Olivier Lacombe and Ioannis Koukouvelas

Received: 19 September 2022
Accepted: 23 November 2022
Published: 29 November 2022

1. Introduction

The literature in this specific field has long postulated that unlike the Alps in the north and the Helenides in the south, there is no lithospheric slab of recent origin underneath the Northern Dinarides [1–3], but only a shallow lithospheric slab to a depth of about 200 km underneath the Southern Dinarides. Ref. [4] suggested that "the asthenospheric upwelling underneath the Pannonian Basin led to a severe modification of a formerly continuous Adriatic lithospheric slab dipping underneath the Dinarides," i.e., subduction effects beneath the Northern Dinarides were removed by the asthenosphere rising in the Miocene. Ref. [3] stated that slab delamination occurred under the Dinarides, and distinguished the slab gap and the north-eastern asthenospheric flow direction beneath the Dinarides.

These considerations are primarily based on certain global and regional seismic tomographic models, as well as the attenuation of a high-velocity anomaly, i.e., fast anomaly, underneath the Dinarides [5–7]. The velocity models [6] and [7] indicate the attenuation of a fast anomaly underneath the Northern Dinarides. However, underneath the Central and Southern Dinarides, there is a shallow fast anomaly, up to 200 km. In the global model of [5], a weak fast anomaly is observed only in the Southern Dinarides. However, recent local tomographic models in the area of the Dinarides [8,9] show the presence of a fast

anomaly underneath the entire Dinarides interpreted as a lithospheric slab dipping into the asthenosphere. Continuous continental subduction under the Dinarides has been also suggested by [10] based on the 3D Pn tomography.

The subduction underneath the Dinarides that occurred in the geological past has already been given [11], but the question of recent deep tectonic processes in the Dinarides can be answered using geophysical methods including modern seismic methods that generate 3D velocity models. The method that particularly stands out is teleseismic tomography, which can discover sinking lithospheric plates and provides answers as to events taking place underneath the Dinarides.

The area investigated using teleseismic tomography covers the Dinarides and marginal parts of the Pannonian Basin. The tomographic model used in determining the lithosphere composition in the Dinarides area has been discussed and analysed in detail [8]. It should be noted that any interpretation process should obey the laws of physics and geology in determining reliable geological models. The basic mistake in interpreting models is simply transposing a geophysical model into a geological model. Although these models appear to be similar, they are based on different fundamental principles and assumptions, which if not taken into account may lead to "pitfalls in seismic interpretation". Seismic forward modelling was performed to provide a geological interpretation of the geophysical 3D velocity model as reliably and accurately as possible, which in turn provides answers to dilemmas regarding the stretching and shape of the Adriatic lithospheric slab underneath the Dinarides.

2. Area of Study including the Regional and Geological Setting

There are three main tectonic units in the surveyed area and surroundings: the Dinarides, Tisza block and Alcapa (Figure 1). The Dinarides are part of the Adriatic microplate which originated from the African plate. The Dinaridic mountain range is situated between the Southern Alps in the northwest and the Hellenides in the southeast, extending approx. 700 km in a NW–SE direction. The Dinarides are usually divided in two units: the External Dinarides, which extend along the Adriatic coast, and Internal Dinarides, as a narrow inland belt. The Tisza block is a separate tectonic segment in the Pannonian Basin which was part of the Eurasian plate. The Alcapa tectonic unit includes the Eastern Alps and Western Carpathians units.

The Dinaridic mountain belt forms a highly complex orogenic system caused by the collision of the African and Eurasian plates. The Adriatic microplate is situated in front of the African plate, which had a role in creating the Alps and Dinarides (Figure 1). It is hypothesised that the Dinarides were created due to the collision between the Adriatic microplate and the Pannonian tectonic segment of the Eurasian plate.

Two ophiolite zones, the Dinaridic which belongs to Internal Dinarides and Sava zones [11–13], are situated between the External Dinarides and the Tisza block. These zones are considered remnants of previous subduction processes and the area is actually a suture zone between the Adriatic microplate and the Tisza block [4,10,13]. The transitional zone between the plates has been identified based on seismic and gravity models devised by [14,15] and is a suture zone. The borders of this zone are shown in the tectonic map given in Figure 1. The boundary of the Tisza block and Alcapa unit is demarcated by the Mid-Hungarian zone (MHZ), which consists of both units. The Dinaridic region is characterised by reverse faulting and the Pannonian Basin is characterised by extending structures [16].

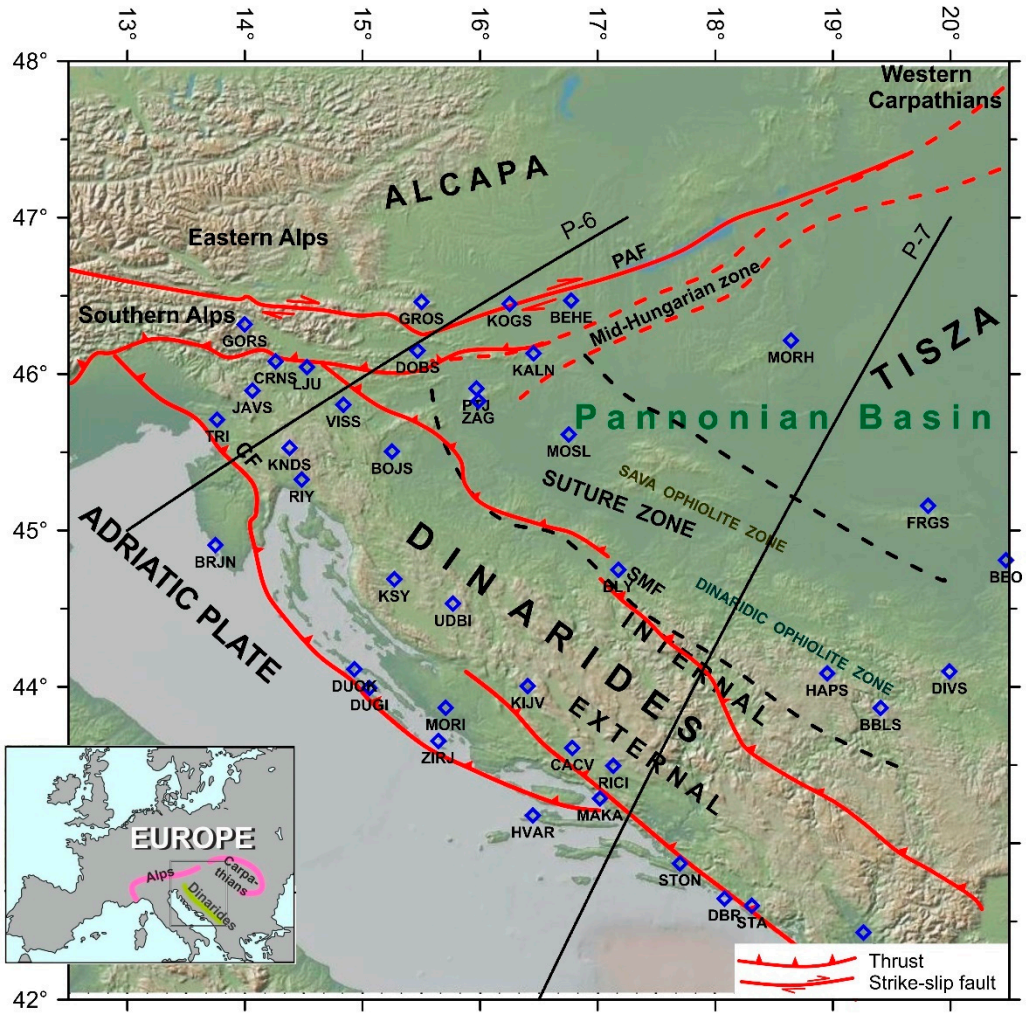

Figure 1. Topographic and position map with tectonics of the Pannonian–Dinaridic including the border area of the Alcapa (Alpine–Carpathian tectonic unit). Permanent seismic stations in the survey area are shown as blue diamonds and the seismic profiles P-6 and P-7 as black lines [8]. The main tectonic units and faults are superimposed on the topographic map (PAF—Periadriatic fault, CF—Ćićarija fault, SMF—South marginal fault of the Pannonian Basin). The borders of the suture zone after [15].

3. An Overview of Adriatic Subduction

Considerations regarding the subduction of the Adriatic microplate underneath the Dinarides were presented after the introduction of the plate tectonics theory [17,18]. Starting from the 1980s and onwards, support was given in academic literature to the subduction model for the Adriatic–Pannonian collision [17], which is somewhat surprising given lacking evidence of any recent subduction, nor evidence of the existence of a descending lithospheric slab in the area. Proof of more recent and active subduction is generally based on the occurrence of both volcanism and deep earthquakes within the Wadati-Benioff zone. However, volcanism has not been observed in recent processes in the Dinarides. Similarly, there are no deep earthquakes, thus seismologists emphasise that all earthquakes occur at shallow depths and only in the Earth's crust [19].

Adriatic subduction as the primary event leading to the formation of the Dinarides was documented in the papers [11,20]. Adriatic subduction is considered a long-term process that lasted from the Upper Jurassic to the Paleogene. Initial subduction processes started in the Late Jurassic and Early Cretaceous periods. The rising of the Dinarides

resulted from strong compressive stresses during the Eocene and the Oligocene periods, and these subduction processes subsequently stopped [11,20,21].

The development of seismic tomography, particularly teleseismic tomography, has led recent geological models in an entirely new direction. The non-existence or attenuation of fast anomalies in tomographic 3D models underneath the Dinarides, or at least in the northern part, has led to the introduction of the concept of a "slab gap" underneath the Dinarides [1,3,5]. On the other hand, [21] introduced a mechanism of a triple junction point to explain the lack of the slab.

Crustal studies in the area of the Dinarides [14,15,22–25] show a strong thickening of the crust underneath the Dinarides and its thinning underneath the Adriatic Sea and Pannonian Basin. Additionally, [26] showed the fast anomaly under the Dinarides in the S-wave velocity model derived from the inversion of the Rayleigh-wave dispersion. This anomaly also indicates lithospheric thickening under the entire Dinarides.

The crust thickness under the Northern Dinarides is about 40 km [14] and increases slightly to 45 km in the Southern Dinarides [15], but decreases to about 20 km underneath the Pannonian Basin and also to 25–30 km in the Adriatic. Similarly, the gravity map shows the gravity minimum extending underneath the entire Dinarides, and thus refers to a thickening of the crust [27]. In general, a gravity map always indicates the relief of the Mohorovičić discontinuity (the Moho layer) at a regional and global scale, which provides the greatest density contrast in the lithosphere [15,28,29]. Therefore, a question arises as to finding an explanation for the thinning of the lithosphere mantle under the Dinarides if the crust is thicker, as already discussed in the mentioned geological model [1]. In other words, if upwelling of the asthenosphere did cause a significant thinning of the lithosphere mantle, why has the crust remained thicker under the Dinarides? This problem is also discussed in the papers [30,31]. From a geological standpoint, it can be said that processes in the crust are somehow connected to processes in the lithosphere mantle. For example, the crust and the lithospheric mantle underneath the Pannonian Basin are thinned, causing the entire Pannonian Basin to become a large geothermal anomaly. However, the model which could explain lithospheric thinning and crustal thickening is lithospheric mantle delamination.

A more logical geological explanation is given by newer local tomographic models that use denser seismic receiver distribution in the Dinarides area [8,9,32,33]. The shallow fast anomaly underneath the Northwest Dinarides can be seen in the model of [32]. A similar fast anomaly is also clearly manifest in the model of [8], which also shows a deep fast anomaly underneath the Southern Dinarides. Similarly, a shallow fast anomaly under the Northern and Central Dinarides, which deepens in the Southern Dinarides, is clearly visible in the P-wave isotropic tomography and P-wave azimuthal anisotropy tomography models of [9]. On the margins of the tomographic model for the Alpine region by [33], and obtained using the finite-frequency tomography method, there is also evidence of a shallow fast anomaly underneath the Northern Dinarides. The similar fast anomaly underneath the Dinarides can be also traced on a recent 3D anisotropic P-wave tomography model [34]. Therefore, recent tomographic models have clearly shown that a fast anomaly exists underneath the entire Dinaridic mountain range that can be seen as the Adriatic lithospheric slab downwelling into the asthenosphere [35].

4. Seismic Network and Resolution

Due to its steep seismic ray paths, teleseismic tomography provides excellent horizontal but low vertical resolution (Figure 2). This can be shown using a simple model where a vertical high-velocity block stretching up to 200 km represents a shallow lithospheric slab. The seismic network, on which the inversion was performed, was taken from [32] and utilised the stations deployed within the project ALPASS-DIPS including several permanent stations situated in the narrow area of the Northern Dinarides [36]. The inverse model shows that the block margins can be accurately determined, hence the horizontal resolution is very good. However, the extension of the block in terms of depth cannot be accurately determined, as is clearly seen in the vertical cross-section. In the inverse model, the block

seemingly extends lengthwise and has a smearing appearance underneath, making the margins along the depth difficult to identify. Consequently, identifying the existence of lithospheric slabs is significantly easier than determining their depth.

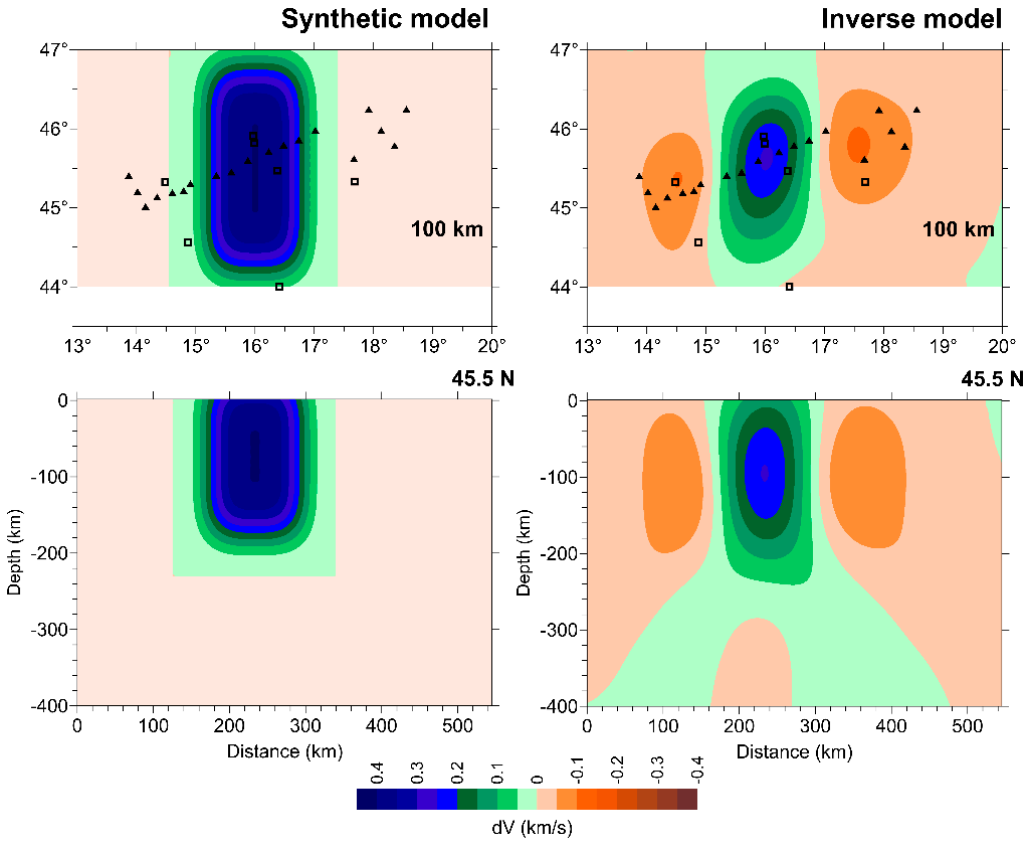

Figure 2. A simple resolution test showing excellent horizontal but poor vertical resolution. The structure, a high velocity block (dV = +0.4 km/s), is shown by the depth slice of 100 km and the vertical cross section of 45.5° N (left side). The inverse model recovered from synthetic travel-time residuals is shown on the right side [32]. Black squares and triangles represent permanent and temporary seismic stations used to collect the observed data.

However, a good horizontal resolution can only be achieved if using a good spatial sampling, along with a sufficient number of samples and an even distribution of seismic stations. Interestingly, [37] showed that a higher number of rays, i.e., the use of a larger number of earthquakes for the same seismic network will not have an influence on the improvement of the inverse model's resolution. Generally speaking, the number of used rays coming from different directions does improve the resolution, and the distribution of stations and data quality or less noise plays an important role, also.

This synthetic seismic model also shows that caution is necessary when interpreting slow anomalies. The existence of only a high-velocity block in the model generates a slow anomaly in the inversion model, even though a low-velocity block does not exist in the initial model (Figure 2). The opposite occurs when only modelling a slow velocity block. This is presumably, at least in part, due to the use of relative arrival-time residuals, resulting in a zero mean of the residuals. Similar features were noticed by [37], meaning the existence of slight deformations in a fast anomaly but prominent artificial features in the form of slow anomalies around a descending lithospheric slab.

Seismic modelling and interpretation are based on the tomographic model obtained by using the seismic network devised by [8], as shown on the gravity map of the area (Figure 3). An additional spike test was carried out to examine the resolution of the used network as is shown in Appendix A. The test clearly shows the structure of the Dinarides can be resolved by applied geometry. The map in Figure 3 indicates seismic stations used in

the models by Piromallo and Morelli [6], PM-model, and Koulakov et al. [7], K-model. It is noticeable that previous models have several stations in the Northern Dinarides and several in the Southern Dinarides, but no stations in the Central Dinarides. The area of the Central Dinarides has been sampled in the recent seismic network [8], SU-model. This model uses 40 seismic stations located in the research area, whereas the PM-model uses 18 stations and the K-model 12 stations. The authors of the PM-model and K-model performed the resolution tests showing also good depth and lateral resolution in this area, achieved by using a higher number of rays and good azimuthal coverage.

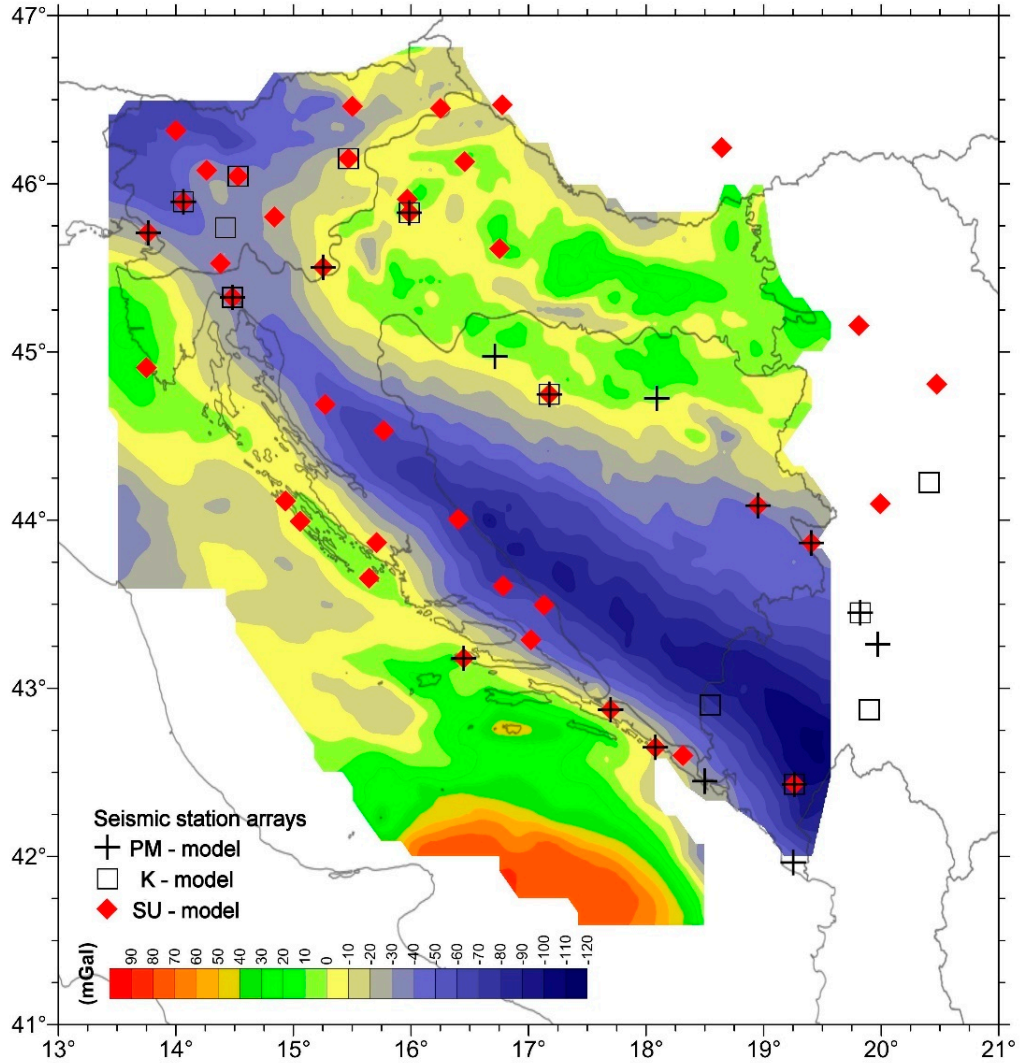

Figure 3. A generalised gravity map of the area of study extracted from [27]. Seismic station networks used in the tomographic models are superimposed and include the PM-model [6], K-model [7] and SU-model [8].

On the other side, the seismic model of [32], which focuses only on the Northern Dinarides, has used a dense network of temporary seismic stations that crosses the Northern Dinarides in the narrowest area. The use of surrounding permanent seismic stations has facilitated identifying the fast anomaly caused by a slab which is narrower than the one in the surrounding mountain massifs, including the Alps and Helenides.

5. Forward and Inverse Problems of the Teleseismic Tomography

On the basis of observed teleseismic data (P-phase), relative travel-time residuals were calculated for use as input data for tomographic inversion. The seismic network consists of 40 seismological stations [8], Figure 4, and seismic events used are in the 30–95° epicentral distance. Distant earthquakes were selected during a period of 24 months (2014–2015), and a set of 90 earthquakes were considered in calculating the P-wave travel-time residuals. The relative travel-time residual for station i is is the difference between the absolute residual (a_i) and mean residual (a_{av}) for the selected earthquake:

$$r_i = a_i - a_{av}. \quad (1)$$

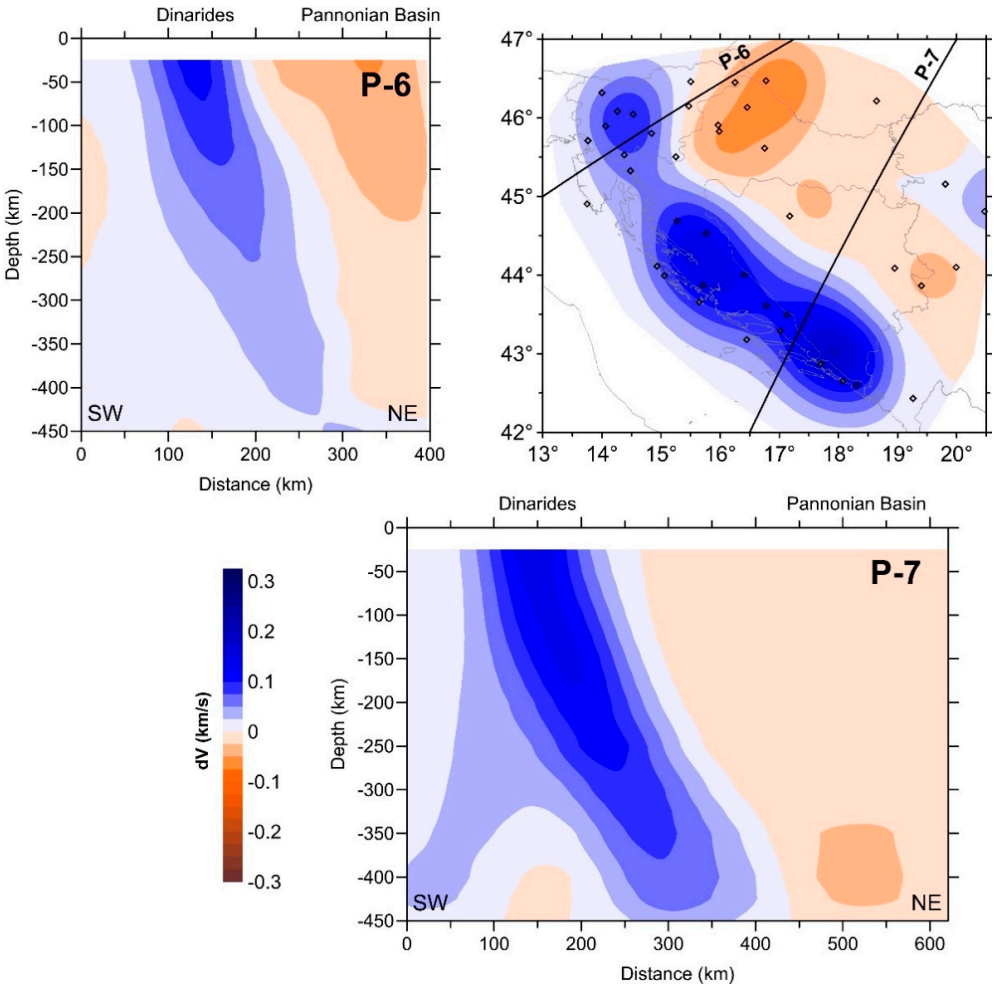

Figure 4. Depth slice at 100 km using the three-dimensional velocity SU-model [8]. Pronounced fast anomaly can be followed in the entire Dinaridic mountain belt. Diagonal cross-sections placed in the Northern and Southern Dinarides (P-6 and P-7) point out the steep fast anomaly beneath the Dinarides probably caused by the descent Adriatic lithospheric slab. Damping of the fast anomaly in the Northern Dinarides is seen on the depth slice.

The absolute travel-time residual is the difference between observed (t_i) and predicted travel times (a_{ip}):

$$a_i = t_i - a_{ip}, \quad (2)$$

The mean residual is:

$$a_{av} = \frac{1}{n}\sum_{i=1}^{n} a_i, \quad (3)$$

where n is the number of observed travel-time arrivals for the earthquake.

Ref. [8] used the adaptive stacking technique to calculate relative travel-time residuals. The method was developed by [38] and [39], while [40] improved this method and nowadays it is among the few methods that are in common usage. The method is robust, insensitive to noise and automatically generates the uncertainty of each calculated residual. The local three-dimensional velocity model was calculated using the inversion method of [41]. A global 1-D *ak135* reference model was used as the initial velocity field [42].

The travel times were calculated for all stations of the seismic array from each distant earthquake and then backtracked by propagation path tracing to the base of the local 3D model. The forward problem was solved using the fast marching method [41], which is a grid-based eikonal solver. The inversion was carried out using the subspace inversion method [43], which projects the full linearised inverse problem onto a much smaller n-dimensional model space. The nonlinearity of the inversion problem was addressed by an iterative procedure, where each step includes the calculation of travel times in the updated velocity model. The inversion procedure stability was achieved by the damping and smoothing parameters.

The 3D grid consisted of 19 radial grid points, separated every 25 km in depth, extending down to 450 km. In a lateral sense, the grid was comprised of 11 nodes in the north–south and 17 nodes in the east–west directions, separated every 0.5°. The origin lies at 47° N 13° E and the volume of the local model consisted of 3553 velocity nodes. Station terms or static corrections for crustal structures were also applied, as the main goal of the teleseismic inversion is to obtain velocity changes in the lithospheric mantle pointing to the relations between the plates in a collision [44]. Calculations of the station terms were carried out by the algorithm of [41] and an additional damping factor ($\varepsilon = 2000$) ensured that only local velocity perturbations were considered.

Forward seismic modelling involves the calculation of a 3D model of seismic velocities for a given geodynamic model represented by 3D synthetic velocity models. In the first step, geodynamic models were constructed in the same local 3D grid as used in the teleseismic inversion of observed travel-time residuals by [8]. The construction of synthetic velocity models was performed using an additional function implemented in used Fast Marching Teleseismic Tomography Package (FMMT software) by Nick Rawlinson. The Adriatic lithospheric slab was represented by the high-velocity blocks beneath the Dinarides (Figures 5–8). In the second step, synthetic travel-time residuals were calculated for a seismic wave travelling through a 3D synthetic velocity model. The third step required inverting the synthetic residuals to obtain a 3D velocity model of synthetic data which was then compared to the 3D inverse model of the observed data. Synthetic travel-time residuals were computed for the same set of receivers and sources as used in the observed data set. Gaussian noises (10%) were also added to synthetic residuals to see the stability of the inversion. The same algorithms and software, which were applied for processing the observed data, were also used in processing the synthetic data [40,41], as well as crustal corrections and damping and smoothing parameters. The inverted images recovered from synthetic travel-time residuals are shown in Figures 5–8 and compared with the inverse model of the observed travel-time residuals from [8].

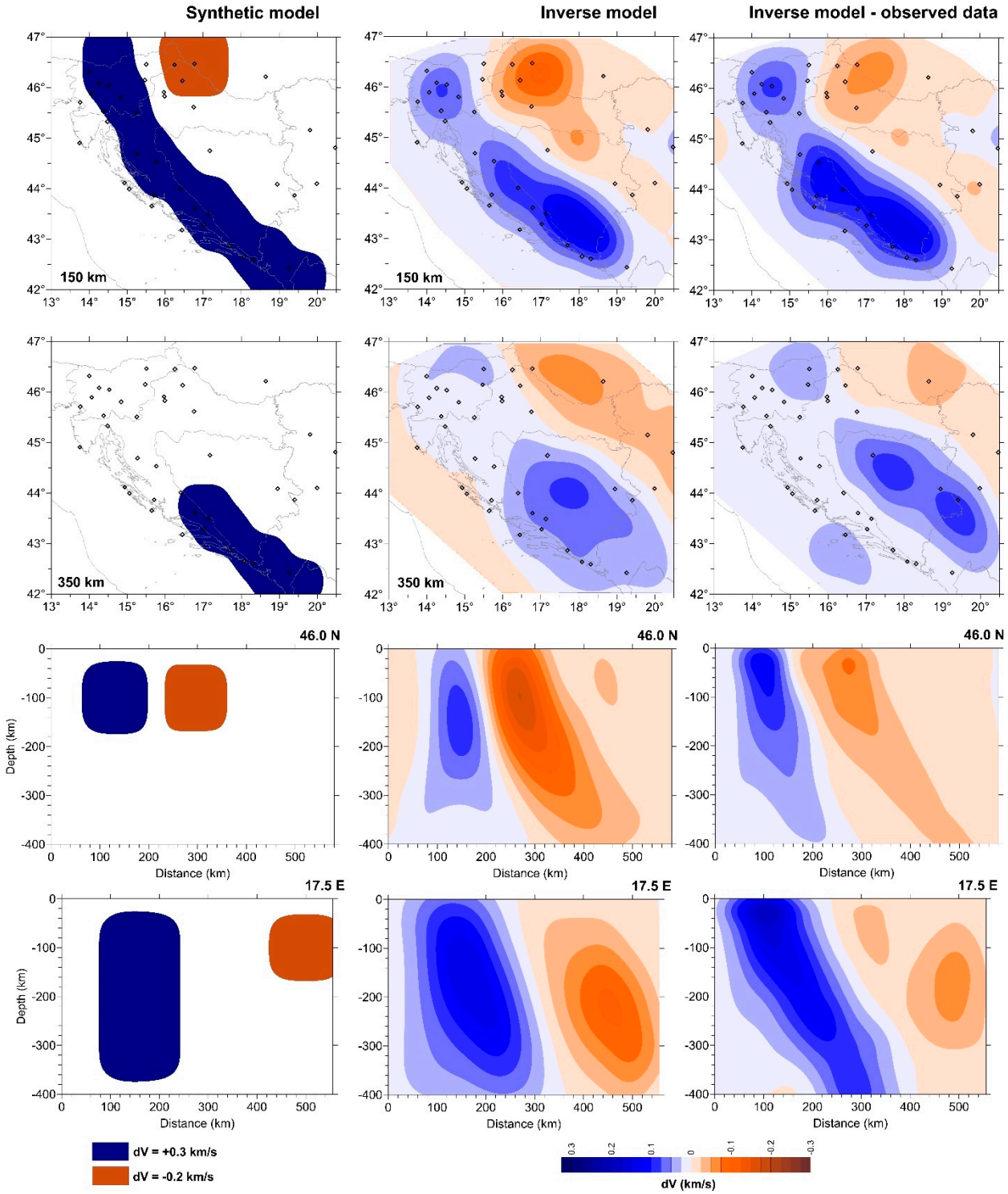

Figure 5. First model. Three-dimensional velocity models showing two depth slices (150 km and 350 km, upper part) and two cross sections (46° N and 17.5° E, lower part). A high-velocity vertical slab in the synthetic model is assumed (left side), where it is shallow in the Northern and deep in the Southern Dinarides. The inverse model recovered from synthetic travel-time residuals is shown in the middle part, and the inverse model of observed travel-time residuals in the SU-model [8] is shown on the right side. Additional low-velocity block is assumed in the Pannonian Basin.

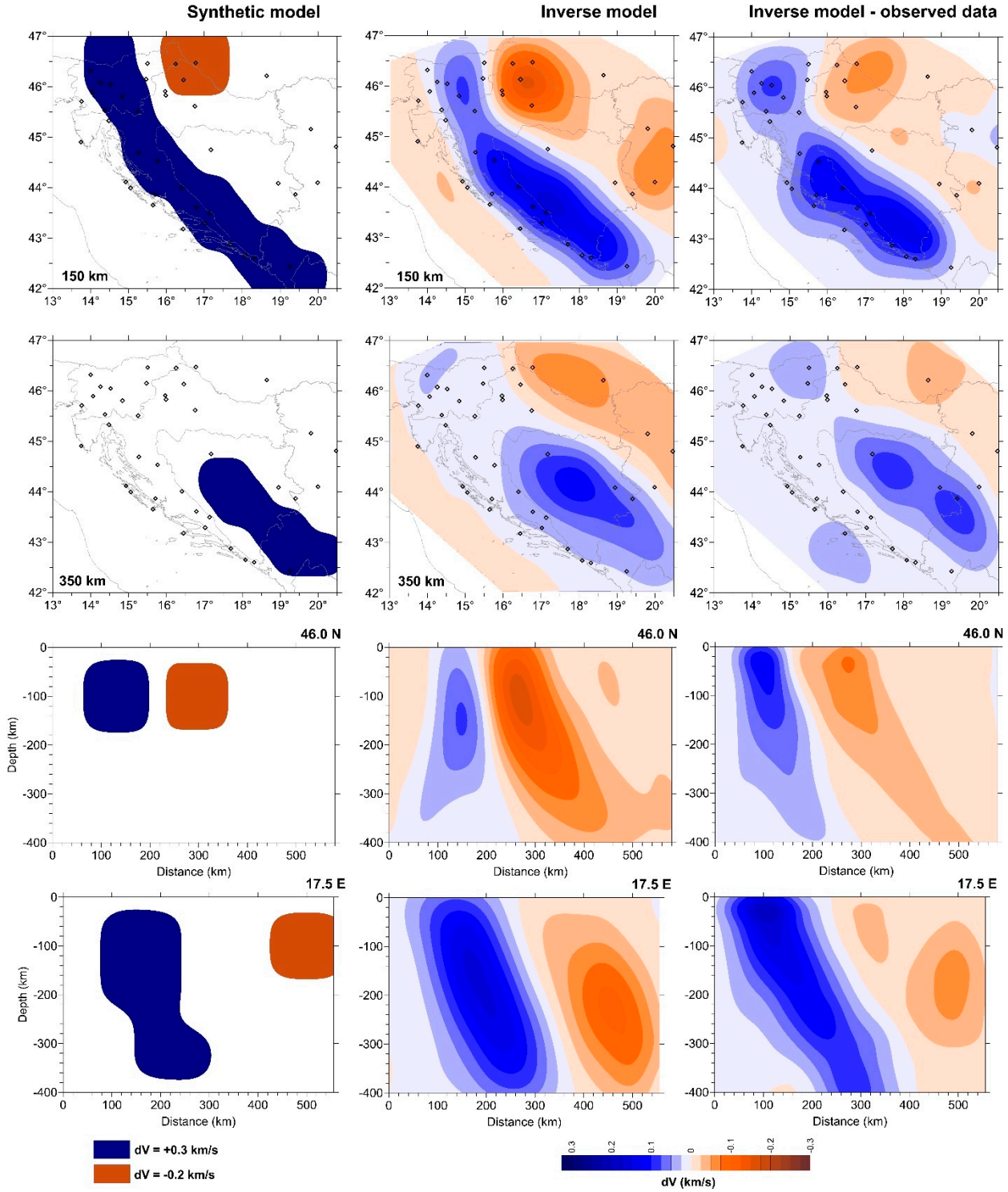

Figure 6. Second model. Three-dimensional velocity models showing two depth slices (150 km and 350 km, upper part) and two cross sections (46° N and 17.5° E, lower part). A shallow high-velocity vertical slab in the synthetic model is assumed in the Northern Dinarides, while deep slab in the Southern Dinarides is divided in two parts, and the deeper part of the slab is shifted towards the northeast (left side). The inverse model recovered from synthetic travel-time residuals is shown in the middle part, and the inverse model of observed travel-time residuals in the SU-model [8] is shown in the right side. Better correlation between the shapes of the anomalies of the inverse models for the synthetic and the observed data than for the first model (Figure 5) can be noticed.

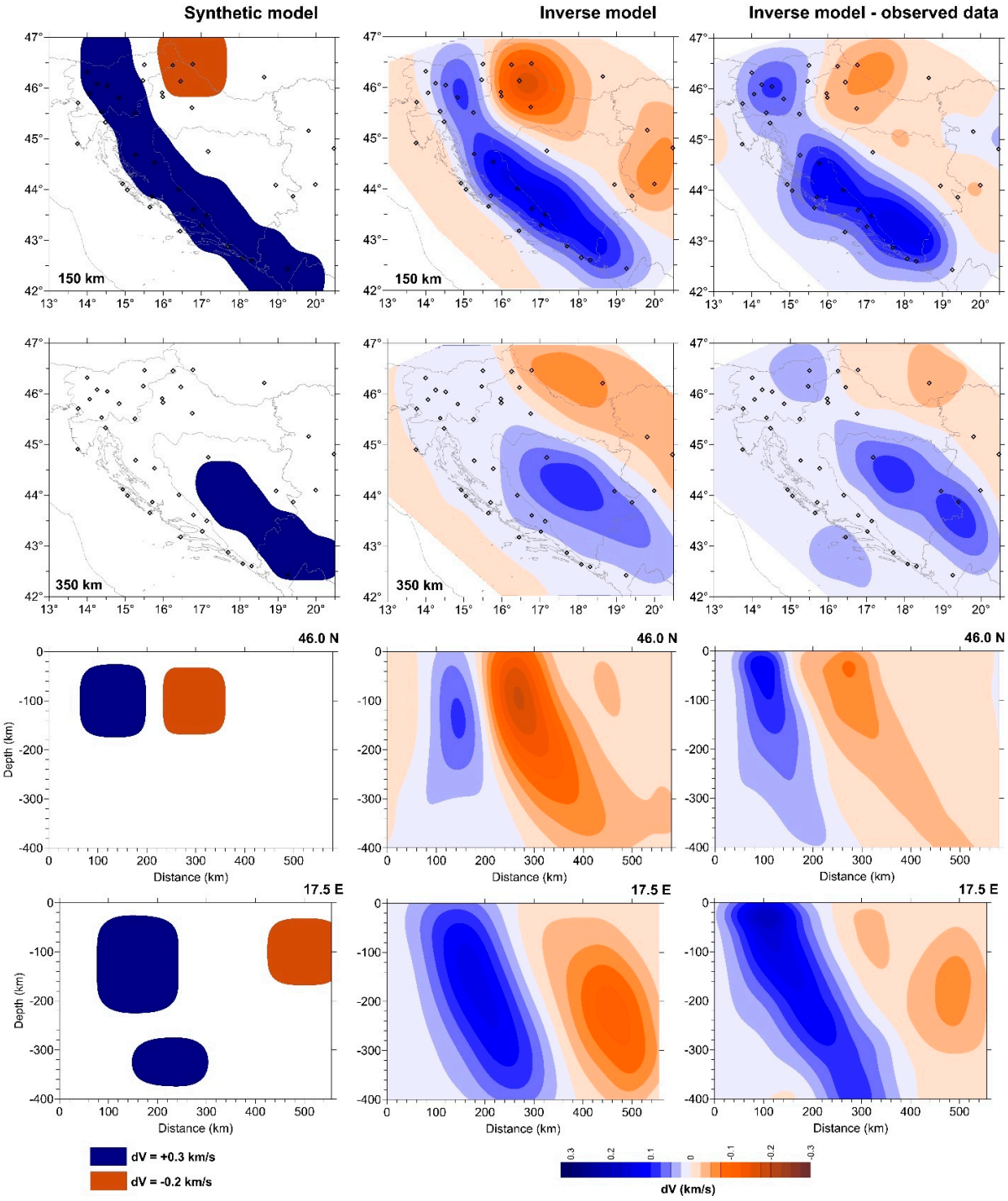

Figure 7. Third model. Three-dimensional velocity models showing two depth slices (150 km and 350 km, upper part) and two cross sections (46° N and 17.5° E, lower part). A shallow high-velocity vertical slab in the synthetic model is assumed in the Northern Dinarides, while deep slab in the Southern Dinarides is divided into two separate blocks, the shallow one and the deep one (left side). The inverse model recovered from synthetic travel-time residuals is shown in the middle part, and the inverse model of observed travel-time residuals in the SU-model [8] is shown in the right side. The correlation between the shapes of the anomalies of the inverse and the observed models is similar (profile 17.5° E) to the second model (Figure 6). Discontinuity in the slab along its depth is difficult to determine due to poor vertical resolution of the method, and deep fast anomaly in the Southern Dinarides cannot be unambiguously interpreted.

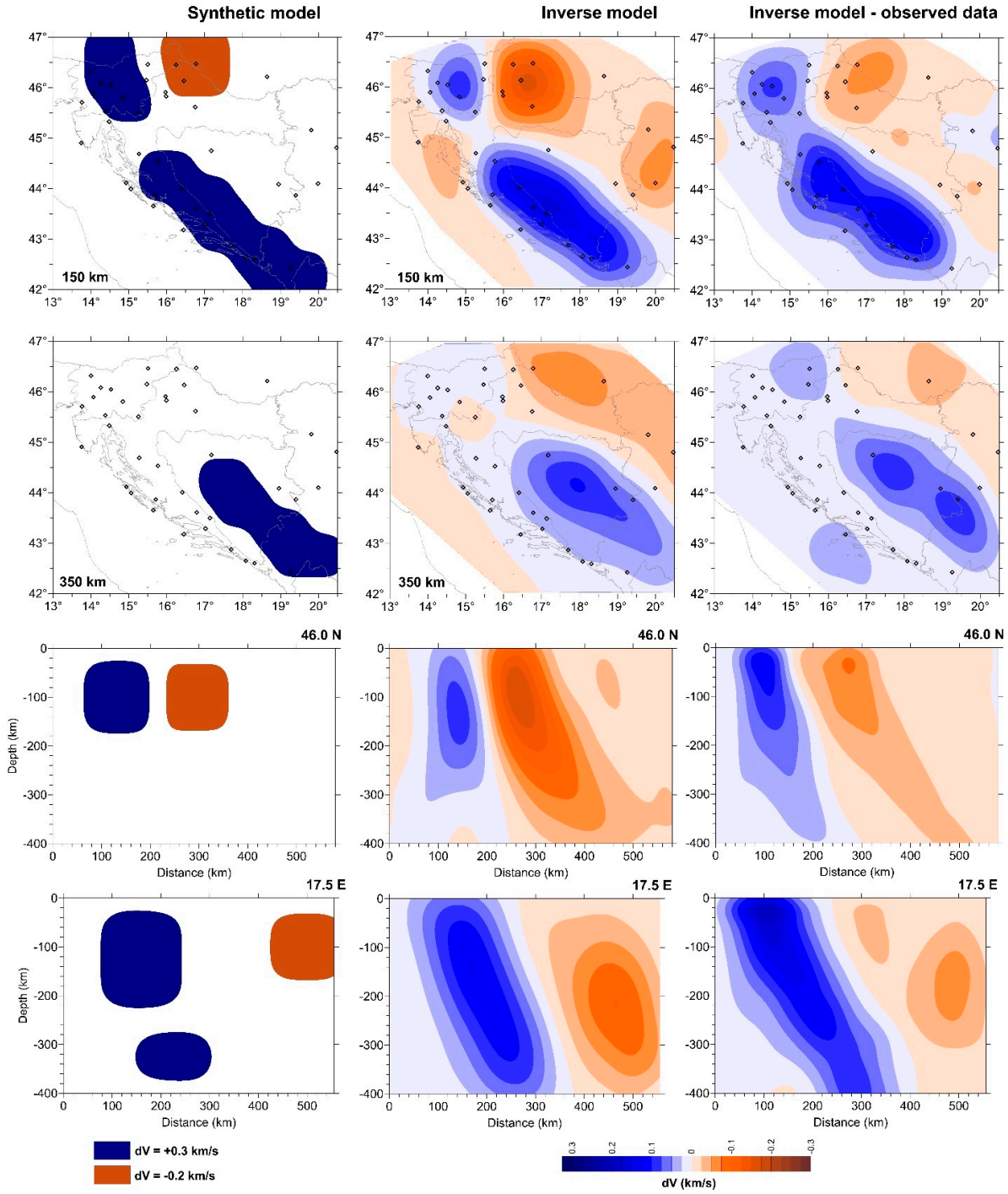

Figure 8. Fourth model. Three-dimensional velocity models showing two depth slices (150 km and 350 km, upper part) and two cross sections (46° N and 17.5° E, lower part). A narrow lateral discontinuity between the Northern and Central Dinarides and two separated blocks in the Southern Dinarides in the deep slab are assumed (left side). The inverse model recovered from synthetic travel-time residuals is shown in the middle part, and the inverse model of observed travel-time residuals in the SU-model [8] is shown on the right side. The shapes of the anomalies of the inverse model for synthetic data have a poor correlation with the shape of the anomalies of the inverse model for observed data, especially seen at depth slices. The slab breakage is pronounced as a discontinuation of the fast anomaly. Therefore, lateral discontinuities in the slab can be very efficiently determined due to good horizontal resolution. Damping of the fast anomaly in the observed model in the Northern Dinarides is the result of the slab geometry and applied seismic network, rather than slab breakage.

6. Seismic Modelling

Based on the fast anomaly underneath the Dinarides, [8] identified a shallow lithospheric slab underneath the Northern Dinarides and a deep slab underneath the Southern Dinarides (Figure 4, the SU-model). However, this model shows a reduced amplitude for the anomaly in the Northern Velebit area (at the start of the Northern Dinarides) and an apparent discontinuity between the Southern and Northern Dinarides (Figures 5–9, the inverse model for the observed data). The first issue is that, at first glance, there seems to be a shallow slab in the Northern Dinarides and a deep slab in the Southern Dinarides, with a discontinuity or at least a strong thinning out of the slab between the two regions. The second issue stems from the earlier mentioned poor vertical resolution of the method. In the Northern Dinarides, a shallow fast anomaly is clearly seen on the transverse profile (Figure 4; P-6), hence the reliable assertion that a shallow lithospheric slab does in fact exist. However, due to poor vertical resolution causing vertical smearing, the question remains as to whether the deep fast anomaly, shown on the transverse profile in the Southern Dinarides (Figure 4; P-7), can be interpreted as a deep continuous lithospheric slab given the actual depth. Hence, detailed seismic modelling was performed to obtain a more reliable geological interpretation of the fast anomaly underneath the Dinarides.

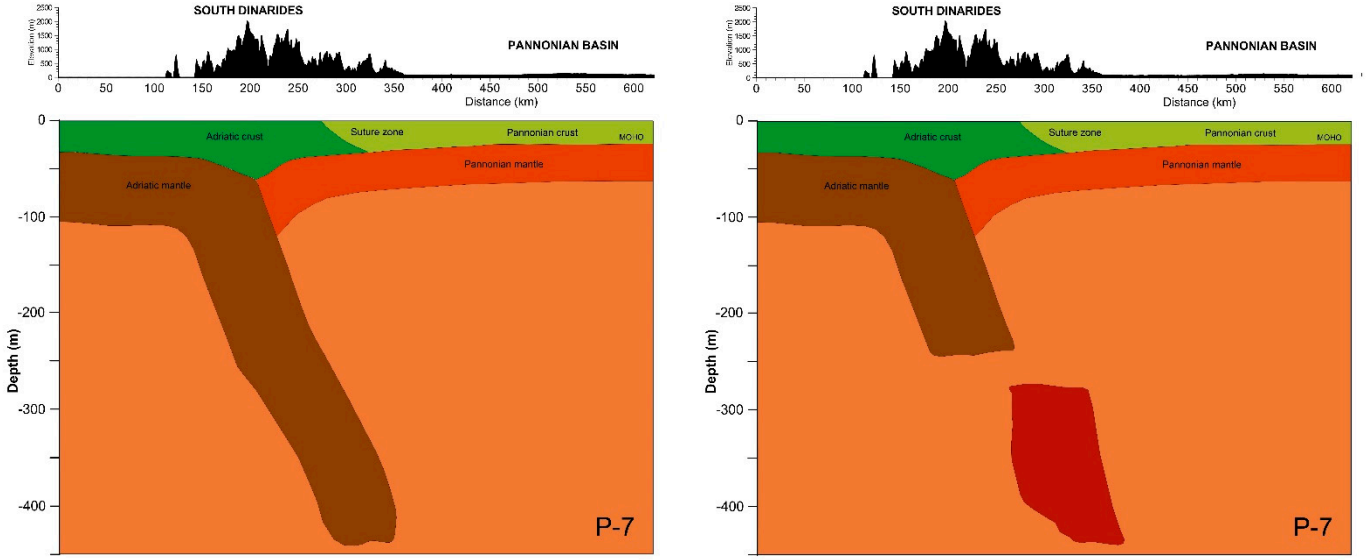

Figure 9. Two possible structural models of the lithosphere in the Southern Dinarides can be devised using forward seismic modelling. The first model (on the left) assumes a steeply dipping continuous Adriatic lithospheric slab [8]. The second model (on the right) presumes that the Adriatic slab consists of two separate blocks, with the deeper block resulting from delamination of the Adriatic lithosphere in a previous subduction. The position of profile P-7 is shown in Figures 1 and 4.

The first synthetic model was devised incorporating a vertically positioned slab with the same width of the fast anomaly along the entire Dinarides, and without any discontinuity (Figure 5). The assumptions were based on the presence of a shallow slab in the Northern Dinarides, and a deep slab to the depth of 400 km in the Southern Dinarides. The velocity anomaly in the sinking slab anomaly is set to a constant value dV = +0.3 km/s in the synthetic model.

To make the synthetic model as realistic as possible, a shallow low-velocity block (dV = −0.2 km/s) is assumed to exist in the marginal south-western part of the Pannonian Basin, underneath the Drava and Sava depression, which stands out in the inverse model for the observed data [8]. This anomaly is also visible in the tomographic model published by [32] and is particularly emphasised by [45] suggesting the upwelling of the asthenosphere in this area.

The inverse model of the input synthetic model shows that the anomaly dampens in the area of the Northern Dinarides, which can be seen on the shallower depth slice at 150 km (Figure 5). This suggests, as does the inverse model for the observed data, the existence of a lateral slab discontinuity at shallow mantle depths, although a continuous slab is obvious in the input synthetic model. Therefore, it becomes evident that slab discontinuity and its slope towards the northeast are only apparent and are caused by the distribution of seismic velocities, the geometry of the slab itself and the distribution of stations and earthquakes, in general, the geometry of measurements. At a deeper depth slice of 350 km, smearing of the anomaly at the northern margin is noticeable, where a fast anomaly appears at depths where the lithospheric slab is no longer present. The smearing in the southern part occurs as a widening of the fast anomaly in the inverse model with increasing depth, whereas the fast anomaly narrows based on the observed data. This is particularly noticeable on the vertical cross-section 17.5 E (Figure 5).

In the second synthetic model, the deep slab in the Southern Dinarides is divided into two parts, where the deeper part of the slab is shifted towards the northeast with respect to the shallower part of the slab, with both parts remaining in contact (Figure 6). In the Northern Dinarides, the shallow slab remains as in the previous model. A better correlation of the shapes of the anomalies exists between the inverse models when compared to the previous model, in terms of synthetic and observed data, and is clearly visible on the depth slices, particularly on profile 17.5 E. This model also demonstrates that the method provides a weaker vertical resolution because the lengthening and smearing of the shallow vertical slab underneath the Northern Dinarides on the inverse vertical cross-section of the profile 46.0 N for synthetic data are visible, similar to the inverse model for the observed data. Therefore, due to the lower vertical resolution provided by the method, determining the slab depth is significantly more difficult than determining horizontal stretching. This is the underlying reason why the author highlights shallow and deep slabs and not their depths.

The slab in the southern part is divided into two separate blocks in the third synthetic model, a shallow and deep slab (Figure 7; profile 17.5 E). The correlation of the shapes of the anomalies between the inverse models, based on the synthetic and observed data is similar compared to the second model, which is best seen in profile 17.5 E. This leads to the conclusion that vertical discontinuity, discontinuity in a slab along its depth, is difficult to determine due to poor vertical resolution. Therefore, the deep fast anomaly in the Southern Dinarides can be interpreted in two ways—as a steeply dipping continuous descending slab, or as a lithospheric slab that consists of two separate blocks.

The previous examples (Figures 5–7) indicate that lateral damping of the anomaly in the Northern Dinarides can be considered only apparent, meaning not caused by a discontinuity of the slab between the Northern and Southern Dinarides. One more seismic model was constructed for the purpose of further investigations. The fourth synthetic model assumes a narrow lateral discontinuity between the Northern and Central Dinarides, meaning between the shallow northern and deep southern lithospheric slabs (Figure 8), while two separated blocks are assumed to exist in the deep slab in the Southern Dinarides. The inverse model clearly shows two separate fast anomalies for the shallow (150 km) depth slice and one fast anomaly in the Southern Dinarides for the deep (350 km) depth slice. The vertical cross-sections show more intense smearing of the shallow fast anomaly in the Northern Dinarides. A correlation of the shapes of the anomalies of the inverse models leads to the conclusion the inverse synthetic model has a weaker correlation with the inverse model for the observed data, which is particularly evident in shallow-depth slices. The lateral discontinuity of the slab in the inverse synthetic model appears as a clear lateral break of the fast anomaly, while such a break does not exist in the inverse model based on observed data, i.e., the fast anomaly is only dampened in one narrow part of the Northern Dinarides. At first glance, one could still say that the differences between the recovered synthetic model and the inverse model of observed data are small. However, there is a small difference in the input synthetic models, that is, a small width of slab gap is assumed. When a larger width is assumed, the differences in the inverse models are

significantly larger. A model with a minimum width of the slab gap is presented here to show that such a boundary model can also be clearly distinguished.

If, however, two connected blocks in the Southern Dinarides are introduced in the synthetic model, it provides a similar inverse synthetic model for the Northern Dinarides, whereas the correlation decreases slightly for the Southern Dinarides. These examples show that lateral discontinuities in the slab, even very narrow slab discontinuities, can be efficiently detected due to the good horizontal resolution provided by the method. This suggests that damping of the fast anomaly in the Northern Dinarides does imply discontinuity of the slab but instead, it can be considered a continuous slab along the entire Dinaridic mountain range. A correct approach is to interpret the data as verifying the existence of a shallow slab in the Northern Dinarides based on [32] due to the dense receiver distribution in the Northern Dinarides.

7. Discussion

Based on previous gravity and seismic data on the crust structure in the Dinarides area and marginal areas [14,15,46] and the seismic models obtained using teleseismic tomography [8,9,32], the valid assertion is that the Adriatic lithosphere mantle undergoes a process of separation from the crust, and then sub-vertically sinking underneath the Dinarides. However, when the lithospheric mantle sinks into the asthenosphere, the lower part of the crust is also frequently pulled down with it. Hence the question remains as to whether this is occurring underneath the Dinarides. Based on teleseismic data, such models are difficult to reliably determine. Using local earthquake tomography from the area of the Northern Dinarides, [46] obtained a narrow slow anomaly in the top part of the upper mantle, located in the north-eastern area of the Dinarides. The anomaly is interpreted as a Moho fragmentation making contact between the European and Adriatic mantles. This anomaly may also indicate that part of the crust is sinking along with the Adriatic mantle. Namely, rocks in the crust are characterised by significantly lower velocities than rocks in the upper mantle, hence a sufficiently large body of crustal rocks in the mantle is identified by a slight decrease in seismic velocities (slow anomaly). However, based on results to date, this is not a reliable conclusion. This question will be the subject of future research. On the other hand, the velocity model based on the P-wave tomographic inversion of the Pn phases can well define the relations in the uppermost mantle. The 3D Pn tomographic model of the Adriatic microplate [10] shows also a low-velocity anomaly (less than 7.6 km/s) underneath the Dinarides which is connected with the slab determined from teleseismic tomography.

The results of forward seismic modelling provide structural models of the lithosphere underneath the Dinarides. This modelling supports the presence of a shallow Adriatic slab that steeply descends under the Northern Dinarides, as already presented in the geological models by [8,9,32]. In previous structural models [8,32], a shallow slab to depths of 220–250 km was interpreted beneath the Northern Dinarides based on the shape of fast anomalies. Seismic modelling, on the other hand, made it possible to consider in more detail the problem of poor vertical resolution of the teleseismic tomography and resulted in the knowledge that the plate can be shallower than in the previous model and will still fit the measured data. After analysing a number of synthetic models, the assessment is that the models with a plate depth in the range of 150–200 km fit best.

However, two models are possible underneath the Central and Southern Dinarides. The first model depicts a deep, steeply dipping continuous Adriatic lithospheric slab, descending to a depth of about 400 km (Figure 9). In the second model, the slab underneath the Southern Dinarides consists of two separated blocks, a deeper and a shallower one. Seismic modelling has shown that none of the models can be preferred. According to the second model, the shallow Adriatic lithospheric slab stretches continuously along the entire Dinarides, with no significant lateral discontinuities in the slab, meaning no slab discontinuity in the Northern Dinarides and no “slab gap” at the depths less than 150 km, but only at greater depths. This border can be at slightly greater depths due to the

poor vertical resolution of the teleseismic tomography. A deeply descending lithospheric slab exists as a separate block of the old Adriatic lithosphere in the Central and Southern Dinarides. The shallow lithospheric slab can be a consequence of recent Adriatic subduction, whereas the deep slab can be considered a remnant of previous, older subduction. In [8], the authors have devised a lithosphere model of the Dinarides based on the deep fast anomaly, while viewing the occurrence of Dinaridic subduction in two phases, which [11] considered to be one long process. The second model (Figure 9), which considers two separate lithosphere blocks in the Southern Dinarides, could point to the theory of two independent subduction phases.

Teleseismic tomography can determine the present structural model of the Dinarides at the level of the lithosphere, but the question of what happened to the subducted oceanic plate [11,12] beneath the Northern Dinarides still remains. It is certainly difficult to believe that the subduction under the Northern Dinarides was much shallower than under the Southern Dinarides because a considerable amount of shortening has been established, which is implicit in the late Cretaceous to Mio-Pliocene thrusting [1,13]. The question of the shallow lithospheric slab under the Northern Dinarides can be solved on the basis of data on the geological development of the Dinarides. Thus, in the literature, the concept of eroding the plate by uplifting the asthenosphere under the Pannonian Basin [1] is considered as opening a gap along the Alps–Dinarides transfer fault which is filled with upwelling asthenosphere [3], also. This event is a consequence of the northwest movement of the Adriatic plate relative to Europe in the post-late Eocene.

The connection between the Alps and the Dinarides could be drawn based on the connection between the shallow fast Dinaridic anomaly and the shallow fast southern Alpine anomaly [2,8]. In both cases, the cause can be the Adriatic lithospheric slab subducting underneath the European slab which in turn is steeply dipping towards the northeast. However, the subduction of the Adria underneath the Alps is still highly debated [47,48]. Four possible scenarios are discussed in paper [47] taking into account the possible subduction of both plates, Adriatic and European, while the second paper [48] favours the model with a single European slab subducted to the south.

Some similarity between the deep fast anomaly underneath the Central and Southern Dinarides, on the one hand, and the deep fast anomaly underneath the Eastern Alps, on the other hand, can be also noticed [2,45,49], and [2,45] identified the existence of a deep lithospheric slab underneath the Eastern Alps and the absence of any fast anomaly, indicating a lithospheric slab underneath the Western and Central Carpathians. A doughnut-shaped fast anomaly underneath the Pannonian Basin at depths from 410 to 660 km, confirmed by [45], has also been observed in other tomographic models [6,7]. This anomaly is often called "the slab graveyard" since it is interpreted as a remnant of previous subductions underneath the Pannonian Basin caused by the delamination of lithospheric slabs. This delamination and the descending of material accumulated during the previous subductions, occurring before the Miocene, [45] is considered to be the cause of the Pannonian extension and the actual origin of the Pannonian Basin. On the other hand, the prevailing hypothesis says that the opening of the Pannonian Basin was caused by the Carpathian roll-back subduction [3]. Furthermore, they have identified [45] a connection between the deep eastern Alpine anomaly with the fast anomaly underneath the Pannonian Basin (Figure 10).

This connection ca be also observed on the southern side of the Pannonian Basin. The deep fast anomaly in the Central and Southern Dinarides [8] could be connected to the deep fast anomaly underneath the Pannonian Basin, visible in Figure 10. The deep fast anomaly from profile P-7 by [8], located in an area not covered by their research data, is situated on profile E by [45]. A possible connection is noticeable between the Dinaridic fast anomaly and the Pannonian deep fast anomaly. Accordingly, these tomographic models can indicate the significant role of Alpine and Dinaridic subductions in the creation of the Pannonian Basin.

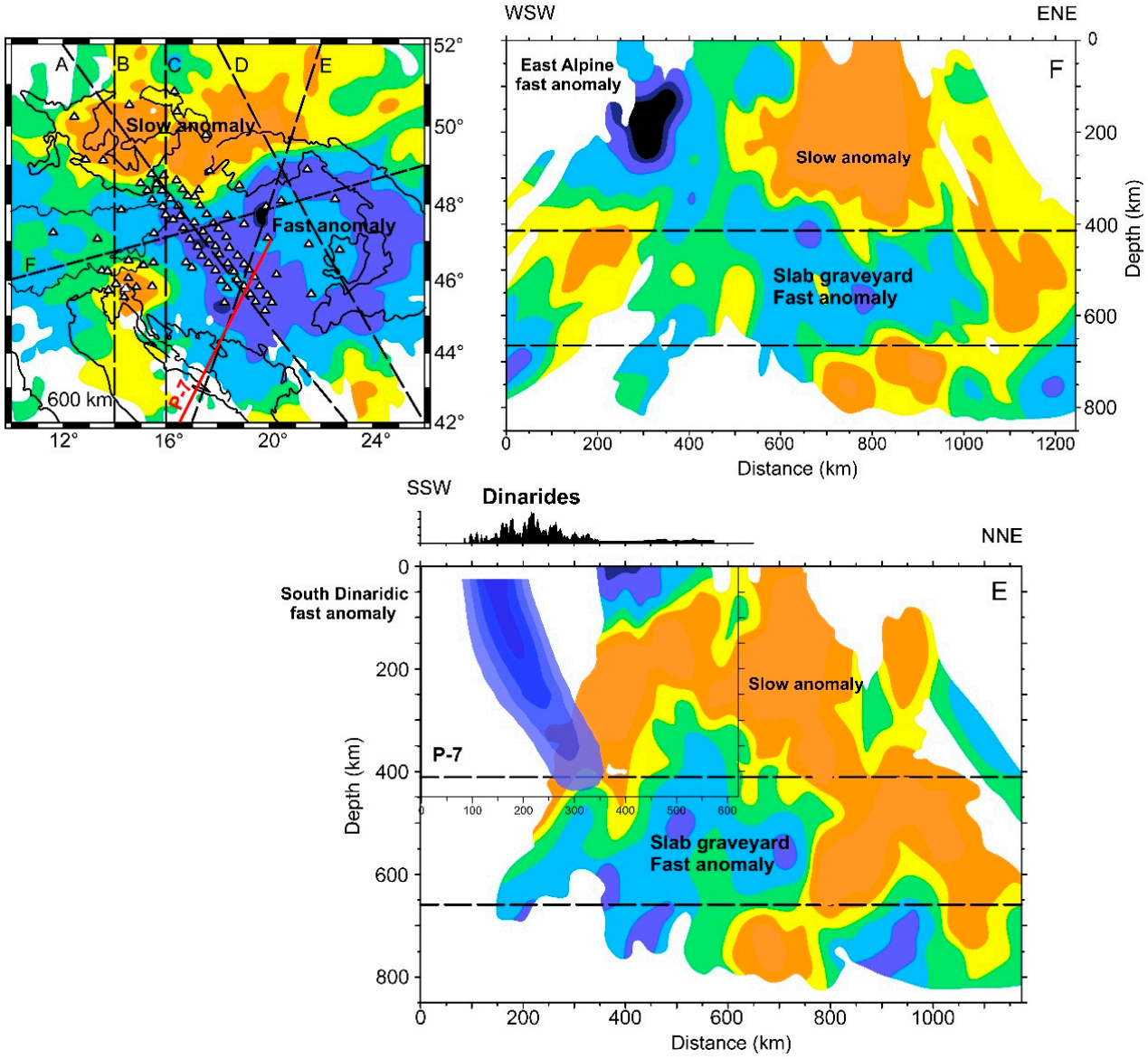

Figure 10. Depth slice at 600 km sketched from the 3D velocity model after [45] showing a donut-shaped fast velocity anomaly underneath the Pannonian Basin. Connection of the East Alpine fast anomaly with this deep fast Pannonian anomaly (slag graveyard) is noticeable on profile F sketch (upper part). The deep fast anomaly in the Southern Dinarides from profile P-7 [8] is situated over profile E sketch after [45] in the lower part. A connection between the Dinaridic fast anomaly and deep Pannonian fast anomaly can be seen.

8. Conclusions

Teleseismic tomography provides a sound definition of interactions in the upper mantle, with a particularly evident downwelling of the solid lithospheric slab into the asthenosphere, which in turn provides the basis for identifying subduction relations. The method exhibits excellent horizontal resolution but poor vertical resolution. This facilitates the detection of potential lithospheric slabs, however, determining their extension depth becomes more difficult. The prerequisite for horizontal resolution is good spatial sampling, primarily density and even receiver distribution and good azimuthal coverage of rays. Recent teleseismic tomographic models [8,9,32,34] were used in discovering the shallow slab underneath the Northern Dinarides and the deep slab underneath the Southern Dinarides. These models achieve good resolution, facilitating more reliable determination

of the fast anomaly underneath the Dinarides, and also the discovery of the Adriatic descending lithospheric slab.

Forward seismic modelling in the Dinarides area has led to a more reliable and more accurate interpretation of the inverse tomographic velocity model by [8]. It shows that the Adriatic slab exists beneath the entire mountain belt of the Dinarides. The slab is shallower underneath the Northern Dinarides (at depths up to 200 km) and deeper underneath the Southern Dinarides (at depths of more than 400 km). Although the inverse 3D velocity model shows damping of the fast anomaly in the Northern Dinarides, seismic modelling shows that the slab is laterally continuous at shallow depths and has similar thickness beneath the entire mountain belt. Therefore, lateral attenuation of the fast anomaly in the Northern Dinarides stems from the actual slab geometry, seismic network and used earthquakes. After conducting the modelling, the author can claim that, indeed, there is no slab gap underneath the Dinarides at depths less than 150 km, but only at greater depths.

Seismic modelling has led to a more reliable and more accurate interpretation of the deep fast anomaly underneath the Southern Dinarides. It shows that the anomaly can be interpreted in two ways due to the poor vertical resolution of the method. In the first model, a steeply dipping continuous Adriatic lithospheric slab descends into the asthenosphere, whereas the second model presents a slab consisting of two separate blocks, meaning that the deeper block results from delamination of the Adriatic lithospheric slab (Figure 9). Due to the similar correlation between the inverse synthetic and observed velocity models for both lithospheric models, preference is not given to any model. The second model could indicate two independent Dinaridic subduction phases, as opposed to viewing subduction as a single long process during the geological past [11,20]. Namely, the shallow Adriatic lithospheric slab, which extends along the entire Dinaridic mountain range, could be considered a consequence of the recent Adriatic subduction, whereas the deep slab could be considered a remnant of the previous, older subduction.

Funding: The exploration was funded by the Ministry of Science and Education of the Republic of Croatia. This work has been also supported by the Virtulab project (KK.01.1.1.02.0022), co-funded by the European Regional Development Fund.

Data Availability Statement: Not applicable.

Acknowledgments: I extend my appreciation to Nicholas Rawlinson who provided the FMTT software on open-source terms. I am also grateful to Editor and anonymous reviewers for their careful and constructive reviews.

Conflicts of Interest: The author declares no conflict of interest.

Appendix A

Resolution test: Spike test has been carried out to further examine the resolution of the 3D velocity model of [8], and the results are presented in the Figure A1. Spike test shows again a good horizontal resolution and weaker vertical resolution, which is clearly pointed out in the manuscript. The test also shows that the structure beneath the Dinarides, which is generally simple, can be resolved by the applied seismic array.

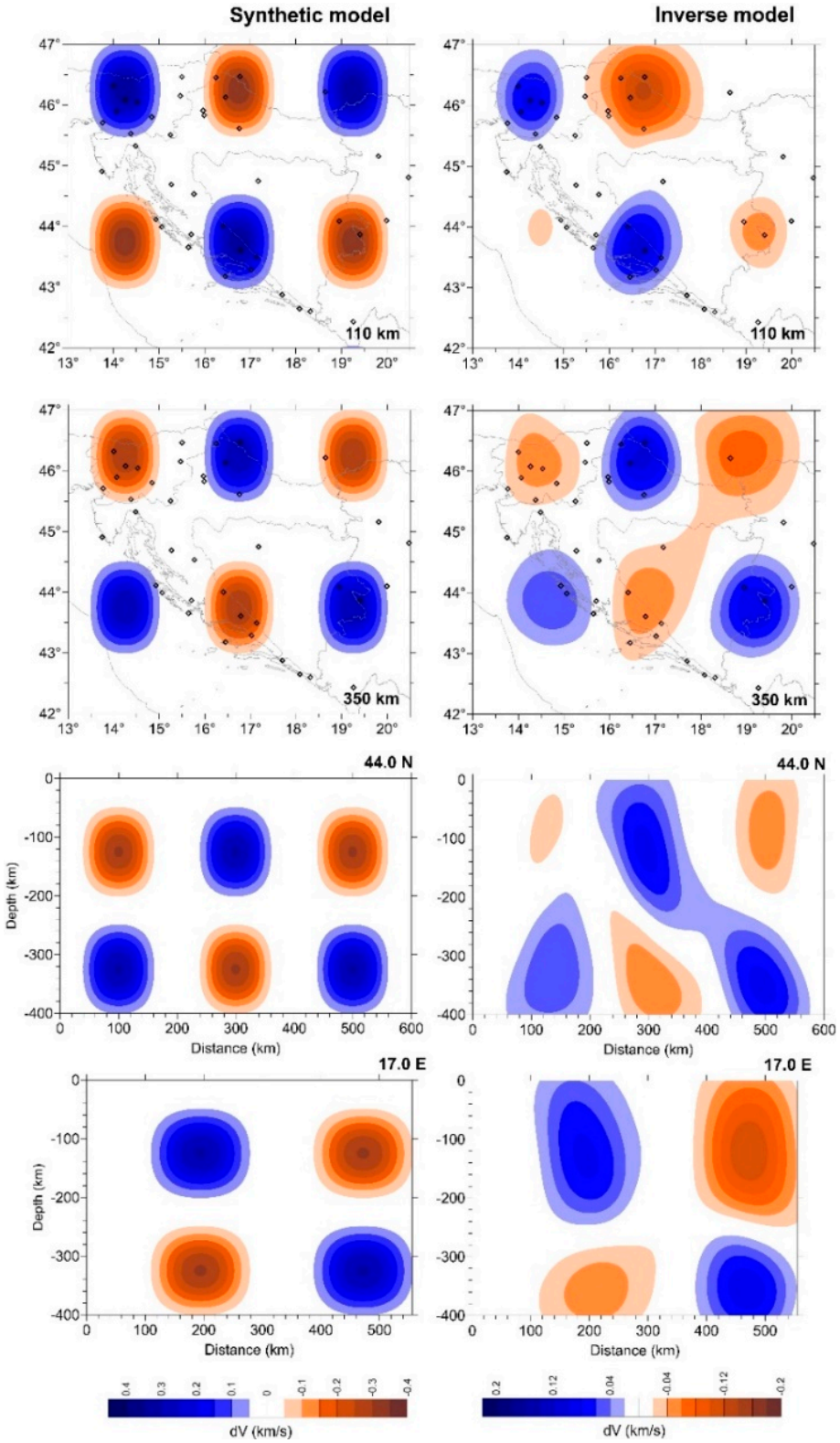

Figure A1. Resolution test—spike test. Positive and negative velocity anomalies (dV = ±0.4 km/s) were superimposed in a regular pattern on the ak135 model and recovered by an inversion with the parameters used for the solution model. A synthetic model is shown together with the inversion slices at 110 km and 350 km (upper part), and at the west–east profile (44.0 N) and south–north profile (17.0 E; lower part). Better resolution is achieved at greater depths. Inversion model shows that applied geometry can resolve the structure of the Dinarides.

References

1. Ustaszewski, K.; Schmid, S.M.; Fügenschuh, B.; Tischler, M.; Kissling, E.; Spakman, W. A map-view restoration of the Alpine-Carpathian-Dinaridic system for the Early Miocene. *Swiss J. Geosci.* **2008**, *101* (Suppl. 1), 273–294. [CrossRef]
2. Mitterbauer, U.; Behm, M.; Brückl, E.; Lippitsch, R.; Guterch, A.; Keller, G.R.; Koslovskaya, E.; Rumpfhuber, E.M.; Šumanovac, F. Shape and origin of the East-Alpine slab constrained by the ALPASS teleseismic model. *Tectonophysics* **2011**, *510*, 195–206. [CrossRef]
3. Handy, M.R.; Ustaszewski, K.; Kissling, E. Reconstructing the Alps-Carpathians-Dinarides as a key to understanding switches in subduction polarity, slab gaps and surface motion. *Int. J. Earth Sci.* **2015**, *104*, 1–26. [CrossRef]
4. Ustaszewski, K.; Kounov, A.; Schmid, S.M.; Schaltegger, U.; Krenn, E.; Frank, W.; Fügenschuh, B. Evolution of the Adria-Europe plate boundary in the northern Dinarides: From continent-continent collision to back-arc extension. *Tectonics* **2010**, *29*, TC6017. [CrossRef]
5. Bijwaard, H.; Spakman, W. Non-linear global P-wave tomography by iterated linearized inversion. *Geophys. J. Int.* **2000**, *141*, 71–82. [CrossRef]
6. Piromallo, C.; Morelli, A. P wave tomography of the mantle under the Alpine-Mediterranean area. *J. Geophys. Res.* **2003**, *108*, 2065. [CrossRef]
7. Koulakov, I.; Kaban, M.K.; Tesauro, M. P- and S-velocity anomalies in the upper mantle beneath Europe from tomographic inversion of ISC data. *Geophys. J. Int.* **2009**, *179*, 345–366. [CrossRef]
8. Šumanovac, F.; Markušić, S.; Engelsfeld, T.; Jurković, K.; Orešković, J. Shallow and deep lithosphere slabs beneath the Dinarides from teleseismic tomography as the result of the Adriatic lithosphere downwelling. *Tectonophy* **2017**, *712–713*, 523–541. [CrossRef]
9. Hua, Y.; Zhao, D.; Xu, Y. P wave anisotropic tomography of the Alps. *J. Geophys. Res. Solid Earth* **2017**, *122*, 4509–4528. [CrossRef]
10. Sun, W.; Zhao, L.; Malusà, M.G.; Guillot, S.; Fu, L.Y. 3-D Pn tomography reveals continental subduction at the boundaries of the Adriatic microplate in the absence of a precursor oceanic slab. *Earth Plan. Sci. Lett.* **2019**, *510*, 131–141. [CrossRef]
11. Pamić, J. North Dinaridic late Cretaceous-Paleogene subduction-related tectonostratigraphic units of southern Tisia, Croatia. *Geol. Carp.* **1998**, *49*, 341–350.
12. Pamić, J.; Tomljenović, B.; Balen, D. Geodynamic and petrogenetic evolution of Alpine ophiolites from the central and NW Dinarides: An overview. *Lithos* **2002**, *65*, 113–142. [CrossRef]
13. Schmid, S.M.; Bernoulli, D.; Fügenschuh, B.; Matenco, L.; Schefer, S.; Schuster, R.; Tischler, M.; Ustaszewski, K. The Alpine-Carpathian-Dinaridic orogenic system: Correlation and evolution of tectonic units. *Swiss J. Geosci.* **2008**, *101*, 139–183. [CrossRef]
14. Šumanovac, F.; Orešković, J.; Grad, M.; ALP2002 Working Group. Crustal structure at the contact of the Dinarides and Pannonian Basin based on 2-D seismic and gravity interpretation of the Alp07 profile in the ALP2002 experiment. *Geophys. J. Int.* **2009**, *179*, 615–633. [CrossRef]
15. Šumanovac, F. Lithosphere structure at the contact of the Adriatic microplate and the Pannonian segment based on the gravity modelling. *Tectonophy* **2010**, *485*, 94–106. [CrossRef]
16. Posgay, K.; Bodoky, T.; Hegedüs, E.; Kovácsvölgyi, S.; Lenkey, L.; Szafián, P.; Takács, E.; Tímár, Z.; Varga, G. Asthenospheric structure beneath a Neogene Basin in southeast Hungary. *Tectonophy* **1995**, *252*, 467–484. [CrossRef]
17. Herak, M. A new concept of geotectonics of the Dinarides. *Acta Geol. Zagreb* **1986**, *16*, 1–24.
18. Moretti, I.; Royden, L. Deflection, gravity anomalies and tectonics of doubly subducted continental lithosphere: Adriatic and Ionian Sea. *Tectonics* **1988**, *7*, 875–893. [CrossRef]
19. Markušić, S.; Gülerce, Z.; Kuka, N.; Duni, L.; Ivančić, I.; Radovanović, S.; Glavatović, B.; Milutinović, Z.; Akkar, S.; Kovačević, S.; et al. An updated and unified earthquake catalogue for the Western Balkan region. *Bull. Earthq. Eng.* **2016**, *14*, 321–343. [CrossRef]
20. Tari, V.; Pamić, J. Geodynamic evolution of the northern Dinarides and the southern part of the Pannonian Basin. *Tectonophy* **1998**, *197*, 269–281. [CrossRef]
21. Brückl, E.; Bleibinhaus, F.; Gosar, A.; Grad, M.; Guterch, A.; Hrubcová, P.; Keller, G.R.; Šumanovac, F.; Tiira, T.; Yliniemi, J.; et al. Crustal structure due to collisional and escape tectonics in the Eastern Alps region based on profiles Alp01 and Alp02 from the ALP 2002 seismic experiment. *J. Geophys. Res.* **2007**, *112*, B06308. [CrossRef]
22. Skoko, D.; Prelogović, E.; Aljinović, B. Geological structure of the Earth's crust above the Moho discontinuity in Yugoslavia. *Geophys. J. Roy. Astr. Soc.* **1987**, *89*, 379–382. [CrossRef]
23. Šumanovac, F. Lithosphere model of the Pannonian-Adriatic overthrusting. *Tectonophy* **2015**, *665*, 79–91. [CrossRef]
24. Orešković, J.; Šumanovac, F.; Hegedűs, E. Crustal structure beneath Istra peninsula based on receiver function analysis. *Geofizika* **2011**, *28*, 247–263.
25. Stipčević, J.; Herak, M.; Molinari, I.; Dasović, I.; Tkalčić, H.; Gosar, A. Crustal Thickness Beneath the Dinarides and Surrounding Areas from Receiver Functions. *Tectonics* **2020**, *12*, 2633–2669. [CrossRef]
26. Belinić, T.; Kolinsky, P.; Stipčević, J.; AlpArray Working Group. Shear-wave velocity structure beneath the Dinarides from the inversion of Rayleigh-wave dispersion. *Earth Plan. Sci. Lett.* **2020**, *555*, 116686. [CrossRef]
27. Šumanovac, F. Gravity map of Yugoslavia. In *Gravimetrijska Karta SFR Jugoslavije—Bouguerove Anomalije, 1:500.000*; Federal Geological Institute: Beograd, Serbia, 1972.

28. Mohorovičić, A. Potres od 8. X 1909. In *Godišnje Izvješće Zagrebačkog Meteorološkog Opservatorija za Godinu*; English translation in 1992, Earthquake of 8 October 1909. Geofizika 9:3-55; WorldCat Publisher: Dublin, OH, USA, 1909; Volume 9, pp. 1–56. (In Croatian)
29. Dragašević, T.; Andrić, B. Deep seismic sounding of the Earth's crust in the area of the Dinarides and the Adriatic Sea. *Geophys. Pros.* **1968**, *6*, 54–76. [CrossRef]
30. Belinić, T.; Stipčević, J.; Živčić, M.; Alp Array Working Group. Lithospheric thickness under the Dinarides. *Earth Plan. Sci. Lett.* **2018**, *484*, 229–240. [CrossRef]
31. Balling, P.; Grützner, C.; Tomljenović, B.; Spakman, W.; Ustaszewski, K. Post-collisional mantle delamination in the Dinarides implied from staircases of Oligo-Miocene uplifted marine terraces. *Sci. Rep.* **2022**, *11*, 2685. [CrossRef]
32. Šumanovac, F.; Dudjak, D. Descending lithosphere slab beneath the Northwest Dinarides from teleseismic tomography. *J. Geod.* **2016**, *102*, 171–184. [CrossRef]
33. Zhao, L.; Paul, A.; Malusa, M.G.; Xu, X.; Zheng, T.; Solarino, S.G.; Guillot, S.; Schwartz, S.; Dumont, T.; Salimbeni, S.; et al. Continuity of the Alpine slab unraveled by high-resolution P wave tomography. *J. Geophys. Res. Sol. Earth* **2016**, *121*, 8720–8737. [CrossRef]
34. Rappisi, F.; VanderBeek, B.P.; Faccenda, M.; Morelli, A.; Molinari, I. Slab Geometry and Upper Mantle Flow Patterns in the Central Mediterranean from 3D Anisotropic P-Wave Tomography. *J. Geophys. Res. Sol. Earth* **2022**, *127*, e2021JB023488. [CrossRef] [PubMed]
35. Malusà, M.G.; Guillot, S.; Zhao, L.; Paul, A.; Solarino, S.; Dumont, T.; Schwartz, S.; Aubert, C.; Baccheschi, P.; Eva, E.; et al. The deep structure of the Alps based on the CIFALPS seismic experiment: A synthesis. *Geochem. Geophys. Geosyst.* **2021**, *22*, e2020GC009466. [CrossRef]
36. Šumanovac, F.; Hegedűs, E.; Orešković, J.; Kolar, S.; Kovács, A.C.; Dudjak, D.; Kovács, I.J. Passive seismic experiment and receiver functions analysis to determine crustal structure at the contact of the northern Dinarides and southwestern Pannonian Basin. *Geophys. J. Int.* **2016**, *205*, 1420–1436. [CrossRef]
37. Bezada, M.J.; Faccenda, M.; Toomey, D.R. Representing anisotropic subduction zones with isotropic velocity models: A characterization of the problem and some steps on a possible path forward. *Geochem. Geophys. Geosyst.* **2016**, *17*, 3164–3189. [CrossRef]
38. Jansson, B.; Husebye, E.S. Application of array data techniques to a network of ordinary seismograph stations. *Pure Appl. Geophys.* **1966**, *63*, 83–104. [CrossRef]
39. Gangi, A.F.; Fairborn, J.W. Accurate determination of seismic array steering delays by an adaptive computer programme. *Suppl. Al Nuovo Cim. Ser.* **1968**, *1*, 105–115.
40. Rawlinson, N.; Kennett, B.L.N. Rapid estimation of relative and absolute delay times across a network by adaptive stacking. *Geophys. J. Int.* **2004**, *157*, 332–340. [CrossRef]
41. Rawlinson, N.; Reading, A.M.; Kennett, B.L.N. Lithospheric structure of Tasmania from a novel form of teleseismic tomography. *J. Geophys. Res.* **2006**, *111*, B023101. [CrossRef]
42. Kennett, B.L.N.; Engdahl, E.R.; Buland, R. Constraints on seismic velocities in the Earth from travel times. *Geophys. J. Int.* **1995**, *122*, 108–124. [CrossRef]
43. Kennett, B.L.N.; Sambridge, M.S.; Williamson, P.R. Subspace methods for large scale inverse problems involving multiple parameter classes. *Geophys. J. Int.* **1988**, *94*, 237–247. [CrossRef]
44. Graeber, F.M.; Houseman, G.A.; Greenhalgh, S.A. Teleseismic tomography of the Lachlan Fold Belt and the Newer Volcanic Province, Southeast Australia. *Geophys. J. Int.* **2002**, *149*, 249–266. [CrossRef]
45. Dando, B.D.E.; Stuart, G.W.; Houseman, G.A.; Hegedues, E.; Brückl, E.; Radovanovic, S. Teleseismic tomography of the mantle in the Carpathian-Pannonian region of central Europe. *Geophys. J. Int.* **2011**, *186*, 11–31. [CrossRef]
46. Kapuralić, J.; Šumanovac, F.; Markušić, S. Crustal structure of the northern Dinarides and southwestern part of the Pannonian Basin inferred from local earthquake tomography. *Swiss J. Geosci.* **2019**, *112*, 181–198. [CrossRef]
47. Kästle, E.D.; Rosenberg, C.; Boschi, L.; Bellachsen, N.; Meier, T.; El-Sharkawy, A. Slab break-offs in the Alpine subduction zone. *Sol. Earth* **2020**, *109*, 587–603. [CrossRef]
48. Handy, M.R.; Schmid, S.M.; Paffrath, M.; Friederich, W.; AlpArray Working Group. Orogenic lithosphere and slabs in the greater Alpine area—Interpretations based on teleseismic P-wave tomography. *Sol. Earth* **2021**, *12*, 2633–2669. [CrossRef]
49. Ren, Y.; Stuart, G.W.; Houseman, G.A.; Dando, B.; Ionescu, C.; Hegedüs, E.; Radovanović, S.; Shen, Y. Upper mantle structures beneath the Carpathian-Pannonian region, Implications for the geodynamics of continental collision. *Earth Plan. Sci. Lett.* **2012**, *349–350*, 139–152. [CrossRef]